Supporting Information

Band engineering and crystal field screening in thermoelectric Mg_3Sb_2

Xiaojian Tan[1,2], Guoqiang Liu[1,2,], Haoyang Hu[1], Hezhu Shao[1,2], Jingtao Xu[1,2], and Jun Jiang[1,2,*]*

[1]Ningbo Institute of Materials Technology and Engineering, Chinese Academy of Sciences, Ningbo 315201, China;

[2]Center of Materials Science and Optoelectronics Engineering, University of Chinese Academy of Sciences, Beijing 100049, China;

E-mail: liugq@nimte.ac.cn, jjun@nimte.ac.cn

S1. Band structure

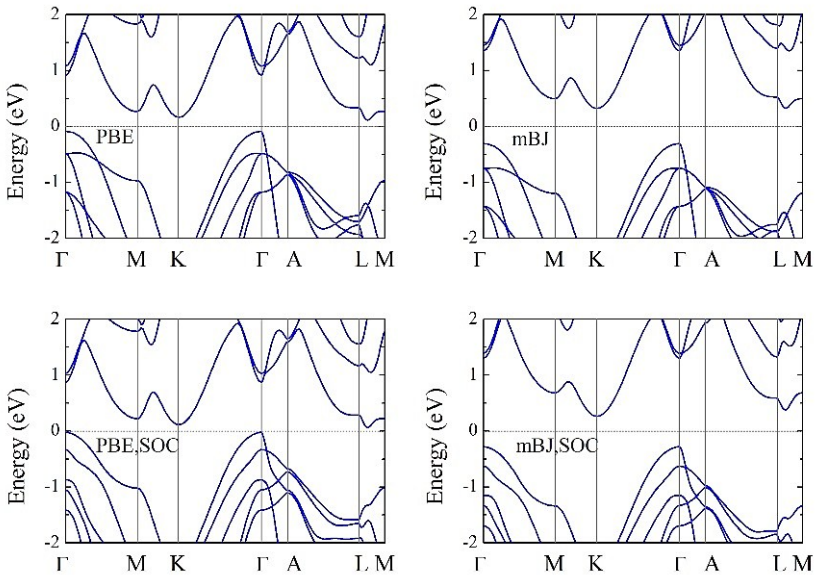

Figure S1. The calculated band structure for Mg_3Sb_2 by using PBE and mBJ functional, without and with spin-orbit coupling (SOC) effect.

S2. First Brillouin zone

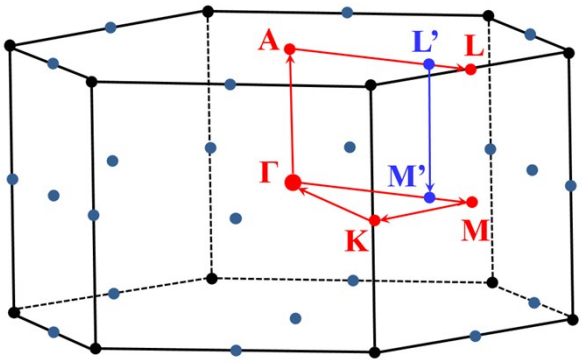

Figure S2. The high symmetry points in the first Brillouin zone of Mg_3Sb_2, and the ***k***-path along Γ-M-K-Γ-A-L and L'(0, 0.417, 0.5) to M'(0, 0.417, 0) are shown.

S3. Band convergence in shrunken Mg_3Sb_2

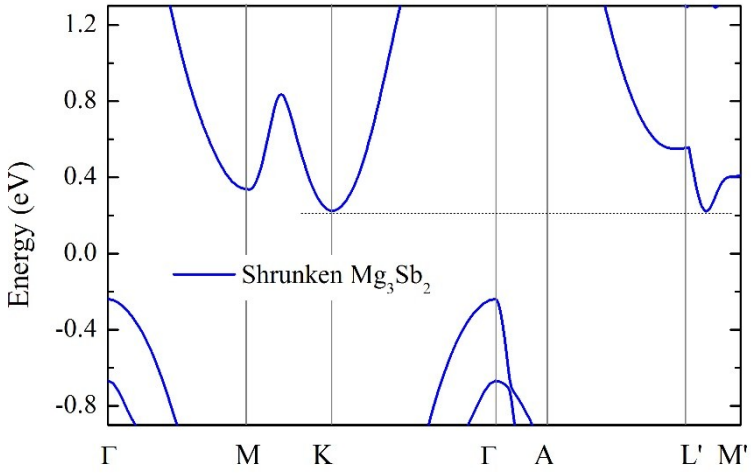

Figure S3. Calculated band structure of shrunken Mg_3Sb_2, and a complete conduction band convergence is achieved.

S4. Band effective mass

Based on the band dispersion of density functional calculations, the effective mass tensor $m_{i,j}^*$ of band edge can be determined by

$$m_{i,j}^* = \frac{\hbar^2}{\partial E(k)^2 / \partial k_i \partial k_j}.$$

For the anisotropic Mg_3Sb_2, the band effective mass then can be calculated by $m_b^* = \sqrt[3]{m_{xx}^* m_{yy}^* m_{zz}^*}$.

The calculated band effective masses and DOS effective masses for the first VBM of Ba-doped Mg_3Sb_2 are summarized in Table S1.

Ba content	m^*_{xx}/m^*_{yy} (m_e)	m^*_{zz} (m_e)	m^*_b (m_e)
0.0	1.143	0.136	0.562
0.125	1.079	0.131	0.534
0.25	1.014	0.127	0.507
0.375	0.926	0.129	0.480

S5. Local structure of Ba-doped Mg_3Sb_2

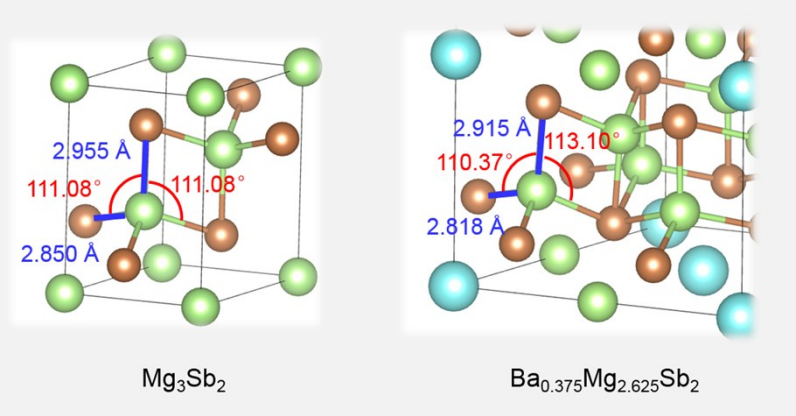

Figure S4. When doping Ba into Mg_3Sb_2, the local structure is little bit changed. Take $Ba_{0.375}Mg_{2.625}Sb_2$ for example, the lattice parameter *a* increases mildly (from 4.606 to 4.690 Å) while *c* increases significantly (from 7.248 to 7.677 Å) relative to pristine Mg_3Sb_2.

S6. Hole mobility

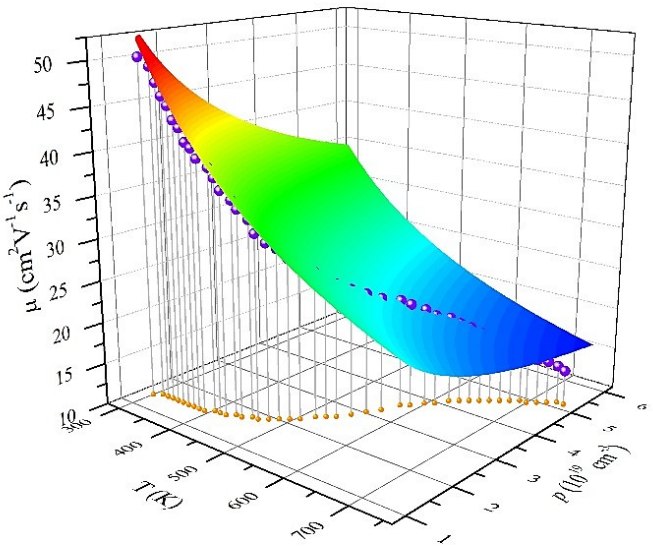

Figure S5. The fitted hole mobility as a function of hole concentration and temperature for *p*-type Mg_3Sb_2, and the experimental results[S1] are also shown for comparison.

S7. Lattice thermal conductivity

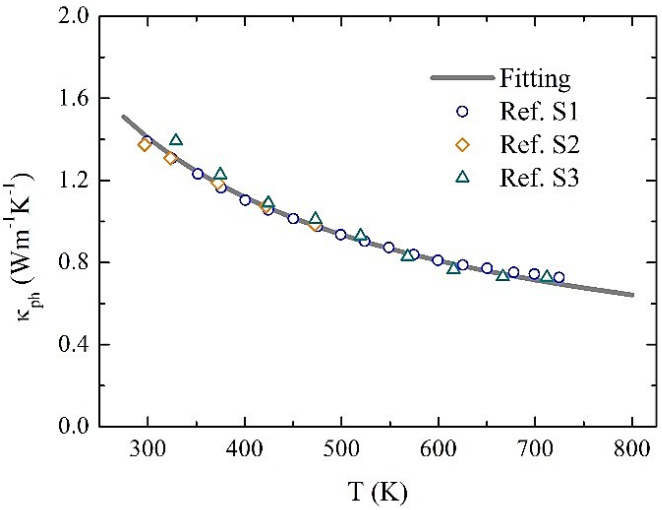

Figure S6. The fitted lattice thermal conductivity as a function of temperature for Mg_3Sb_2, and the experimental results[S1,S2,S3] are also shown for comparison.

References

[S1] L. Song, J. Zhang, B. B. Iversen, Simultaneous improvement of power factor and thermal conductivity *via* Ag doping in *p*-type Mg_3Sb_2 thermoelectric materials, *J. Mater. Chem. A* 5 (2017) 4932–4939.

[S2] Z. Ren, J. Shuai, J. Mao, Q. Zhu, S. Song, Y. Ni, S. Chen, Significantly enhanced thermoelectric properties of *p*-type Mg_3Sb_2 *via* co-doping of Na and Zn, *Acta Mater.* 143 (2018) 265–271.

[S3] H. Tamaki, H. K. Sato, T. Kanno, Isotropic conduction network and defect chemistry in $Mg_{3+}Sb_2$-based layered Zintl compounds with high thermoelectric performance, *Adv. Mater.* 28 (2016) 10182–10187.